ISSN (Print) 1226-1750
ISSN (Online) 2233-6656
Journal of Magnetics 31(2), 250-258 (2026) https://doi.org/10.4283/JMAG.2026.31.2.250

Local Loss Evaluation of Assembled Stator Cores for Electric Vehicles

Long Chen[1,2,3], Xiaoyi Qiao[1], Tong Ben[1,2]*, Hainan Huang[1], Bin Wang[4], and Guanglin Li[5]

[1]*College of Electrical Engineering and New Energy, China Three Gorges University, Yichang 443002, Hubei Province, China*
[2]*Hubei Provincial Research Center on Microgrid Engineering Technology (China Three Gorges University), Yichang 443002, Hubei Province, China*
[3]*Hubei Provincial Engineering Technology Research Center for Power Transmission Line, China Three Gorges University, Yichang, 443002, China*
[4]*Shougang Zhixin Electromagnetic Materials (Qian'an) Co., Ltd., Qian'an, 064400, China*
[5]*Shougang Zhixin Electromagnetic Material Technology (Suzhou) Co., Ltd., Suzhou, 215000, China*

(Received 4 December 2025, Received in final form 2 February 2026, Accepted 2 February 2026)

The magnetic properties of the motor stator core exert a direct influence on its operational efficiency, with residual stresses introduced during the manufacturing process identified as critical factors affecting core losses. Traditional one-dimensional magnetic characterization methods are limited by the complex geometry of the stator. This limitation prevents their direct application for evaluating the local magnetic properties of the assembled core, thereby hindering research into the mechanisms influencing residual stresses on iron loss. To address this limitation, a novel local loss tester was designed and implemented. Following validation of its feasibility through finite element simulation, the device was employed to systematically measure the loss distribution across different depths and magnetization directions within the core under alternating magnetic fields. These measurements revealed axial loss variations attributable to the inherent magnetic anisotropy of non-oriented silicon steel sheets. Comparative studies indicated that traditional one-dimensional methods may introduce measurement deviations as high as 25%. A significant reduction in core losses (approximately 20%) was observed following stress-relief annealing. The effectiveness and reliability of the device were confirmed (relative standard deviation <1% in repeatability tests). This research provides key experimental evidence for the precise assessment of residual stress effects and optimizing stator core design and manufacturing processes.

Keywords : motor stator cores, localized magnetic properties, FEM Simulation, Magnetostriction

1. Introduction

With the increasing global attention to environmental protection and energy sustainability, electric vehicles (EVs) have become an increasingly important solution for clean energy transportation [1-3]. As the core component of electric vehicles, the efficiency and performance of electric motors directly determine the energy-saving and environmental characteristics of the entire vehicle. Therefore, to improve motor efficiency, it is urgent to establish a refined motor manufacturing method that fully considers the impact of process stresses. This is of great engineering value for the development of high-efficiency motors. Against this background, it is crucial to effectively evaluate the local loss properties of the stator core after assembly [4].

Conventional one-dimensional (1-D) magnetic measuring techniques, such as the Epstein Frame (EF) and the Single Sheet Tester (SST), are exclusively applicable to non-processed silicon steel laminations or standardized stacked specimens [5]. These methods demonstrate limited capability in accurately quantifying the loss characteristics of stator cores with complex geometric topologies. Given the inherent magnetocrystalline anisotropy of non-oriented silicon steel, measurement data obtained under 1D magnetization fail to effectively represent the spatial distribution of losses under multi-directional flux paths in actual cores [6, 7]. Crucially, non-uniform residual stress fields generated within electrical steel during manufacturing processes, specifically plastic deformation from stamping operations, assembly stresses during lamination stacking, and thermal residual stresses from welding consolidation,

*Corresponding author: Tel: +86 13820296113
e-mail: bentong@ctgu.edu.cn

significantly alter magnetic domain configuration and dynamic behavior. Consequently, systematic discrepancies arise between conventionally measured results and operational loss properties [8-10]. The fundamental limitation of conventional measurement methods in evaluating processed stator cores stems from their inability to quantitatively characterize the coupled effects of manufacturing-induced residual stress fields and the material's inherent magnetic anisotropy on core loss performance. In recent years, multiple methodologies for evaluating the magnetic properties of assembled stator cores have been developed. In Ref. [11], a rapid measurement technique based on a modified toroidal testing method has been proposed, enabling the quantification of hysteresis loops and core losses in generator stator cores across both laminated and assembled states. Obtained results show that permeability is reduced by 23% and average core losses are increased by 5% due to stamping, compression, and welding processes. An internally excited C-shaped magnetizer has been designed in Ref. [12-15], where bulk loss is evaluated by establishing a closed magnetic circuit with the stator core.

Further, a virtual rotor technique has been introduced to generate rotating magnetic fields for simulating operational conditions [16]. This approach revealed that the actual core loss in industrial motor stator cores exceeds EFmeasurements by 65%, a discrepancy attributed to manufacturing-induced residual stresses. Additionally, a novel stator core loss tester was designed [17], utilizing finite element modeling to quantify, for the first time, the consistent proportion whereby the tester's intrinsic losses constitute 20% of the total measured loss. This quantification thereby provides a reliable method for loss separation in industrial quality inspection. However, all methods mentioned above focus exclusively on tooth-back regions, which suffer from insufficient spatial resolution for the precise characterization of localized core losses.

This paper proposes a method for evaluating the magnetic properties of motor stator cores based on Localized Loss Testing (LLT). The feasibility of this measurement scheme was systematically assessed through finite element numerical simulation and experimental validation. Using the experimental setup, the loss characteristics of the stator teeth and yoke were quantitatively characterized at various spatial angles. Additionally, a comparative analysis was conducted on the hysteresis loop shape and loss characteristic parameters of the core material before and after annealing treatment, confirming that annealing effectively suppress the degradation of magnetic properties caused by residual stress. To verify system reliability, the repeatability of the device was assessed using a dedicated measurement method. The results indicated a low relative standard deviation, demonstrating high reliability.

2. Measurement System and Principle

To assess the local losses in the assembled stator core, a testing setup was developed to evaluate magnetic characteristics, which incorporated a digital feedback device, as depicted in Fig. 1. The system consists of the following components: an NI-branded multifunctional data acquisition card, a power amplifier, voltage and current probes, an SR560 preamplifier, and magnetic yokes designed explicitly for measuring motor stator cores.

Initially, the magnetization signal is generated by a 16-bit data acquisition card. This signal is subsequently amplified via a power amplifier and transmitted to the excitation coil, thereby facilitating the magnetization of the local stator core. Following this, the excitation current and the induced voltage are captured using a voltage probe and a current probe. After the noise reduction by the preamplifier, the data is transmitted to the control program via the data acquisition card for further processing. Through the closed-loop control mechanism, the magnetic flux density associated with the measured loss is strictly controlled as a standard sine wave. The specific control loop architecture is shown in Fig. 2.

The tester features an anti-series double C-type yoke design, with dimensions corresponding to the number of turns of the excitation coil. By utilizing the mutual cancellation effect between the yokes, it effectively suppresses the secondary flux and induced currents in the stator, significantly reducing the measurement error of iron loss. The excitation coil is wound around the outer surface of the magnetic yoke to provide local excitation to

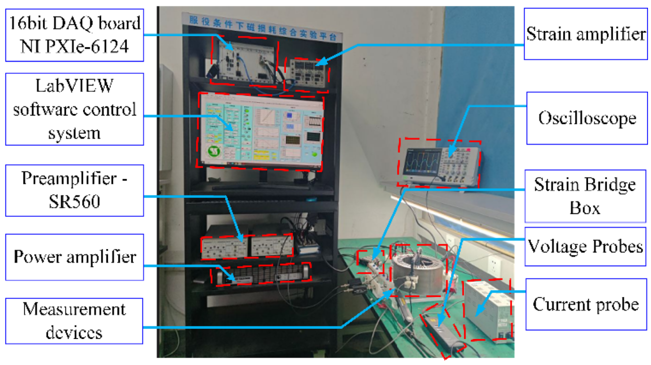

Fig. 1. (Color online) Localised stator loss measurement system for electric motors.

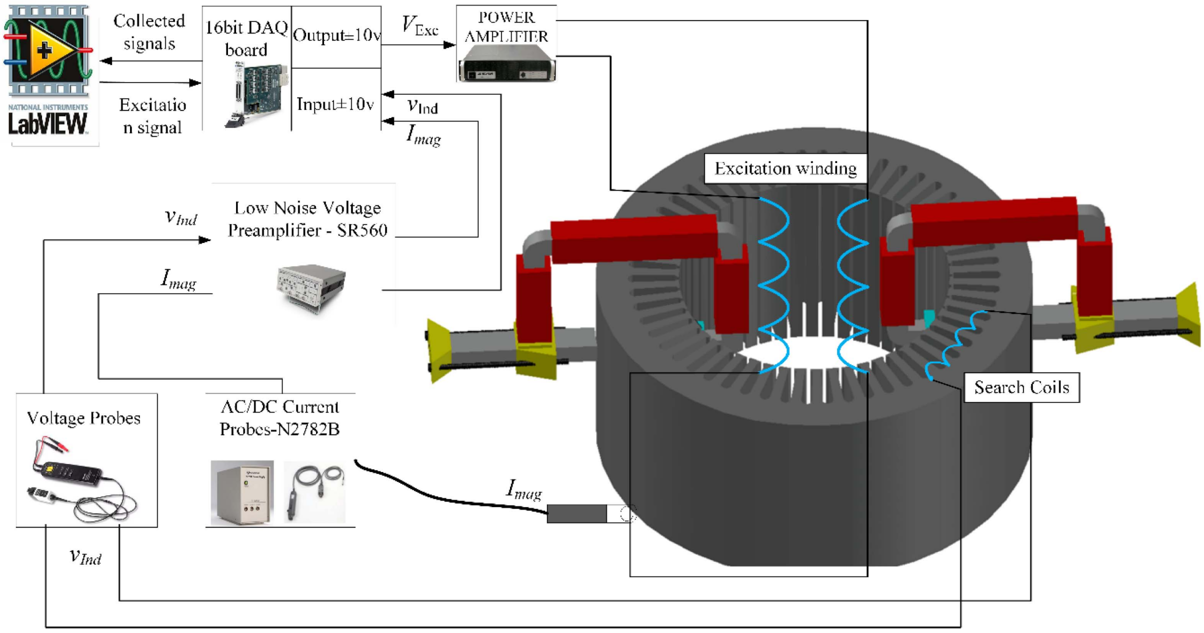

Fig. 2. (Color online) Design and implementation of the hardware control loop architecture for a motor stator loss measurement system.

the motor core, with the magnetic field strength calculated based on the excitation current. The induction coil is wound around the inner surface of the magnetic yoke, generating an induced voltage used to calculate the magnetic flux density. Considering that leakage flux would cause the measured magnetic flux density and magnetic field strength to be overestimated, leading to inaccurate loss measurements, the cross-sectional shape of the measuring device is designed to closely conform to the stator's circular arc. This minimises measurement errors. The specimens and measurement equipment required for testing are shown in Fig. 3. The silicon steel material used in the LLT apparatus is of the same grade (20SW1200) as that fabricated for the stator core of the motor under test. The yoke body is securely fixed to the teeth and back of the motor stator through a precision fixing mechanism. This design aims to minimize the air gap and ensure the maximum tight fit between the yoke and the core, thereby reducing the impact of the air gap on flux measurement. The C-type yoke is equipped with an excitation winding, which generates a uniform magnetic field applied to the motor stator sample. This magnetic field causes the flux lines to pass through the yoke and the core under test, forming a closed magnetic circuit. Additionally, a search coil is wound around the C-type yoke to measure the *B* of the sample.

This study applied three-dimensional finite element analysis (3D FEM) to characterize the magnetic properties of the stator core by evaluating its internal magnetic flux density distribution. This approach facilitated

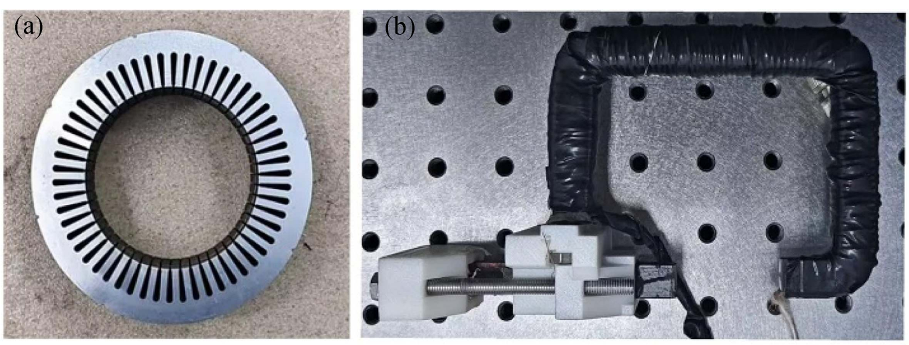

Fig. 3. (Color online) Test specimen and single C-type yoke. (a) Picture of stator core stamped and welded from 20SW1200 non-oriented electrical steel. (b) Measurement equipment diagram.

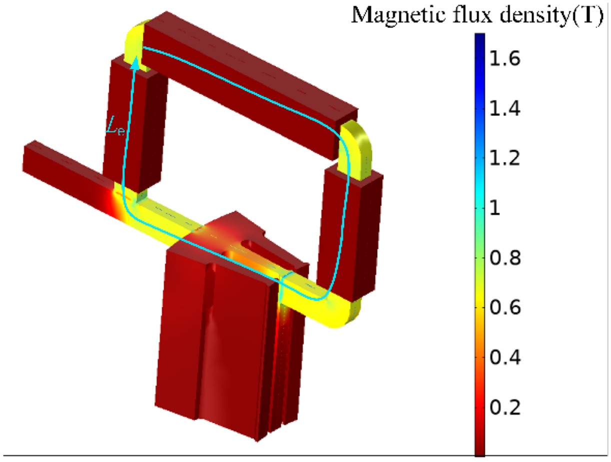

Fig. 4. (Color online) Three-dimensional magnetic field distribution simulation diagram (at Iex = 2 A).

derivation of the magnetic path length (Le). Simulation conditions comprised a 50 Hz excitation frequency, 2 A excitation current, and a uniform 150-turn excitation coil. The resultant 3D magnetic field distribution is depicted in Fig. 4. Le constitutes the aggregate length of the stator tooth, yoke back, and C-shaped yoke sections.

In the electromagnetics measurement of the motor stator sample, the magnetic field strength can be calculated based on Ampere's law, while the magnetic flux density can be determined through Faraday's law of electromagnetic induction. The relevant calculation formulas are as follows:

$$\begin{cases} B(t) = -\dfrac{1}{N_2 S_{\text{sam}}} \displaystyle\int_0^t v_{\text{get}}(t)\mathrm{d}t \\ H(t) = \dfrac{N_1}{L_e} i_{\text{mag}}(t) \end{cases} \tag{1}$$

Where N_1 and N_2 denote the turns of the excitation and induction coils, respectively, S_{sam} represents the sample cross-sectional area, and L_e is the average magnetic path length of the LLT. Local losses are then calculated from the measured flux density B and magnetic field strength H:

$$P_s = \frac{1}{\rho T}\int_T H \cdot \frac{\mathrm{d}B}{\mathrm{d}t}\mathrm{d}t \tag{2}$$

Where P_s is the measured loss value, ρ is the material density, and T is the measurement period.

3. Results and Discussion

3.1. Measurement repeatability verification

To characterize the measurement repeatability of the LLT method, a repeatability assessment procedure was implemented. Seven independent measurements were performed sequentially at an identical test location on the motor stator core under preset flux density levels. The standard deviation of the mean values was calculated based on the measurement data, and the expression is as follows:

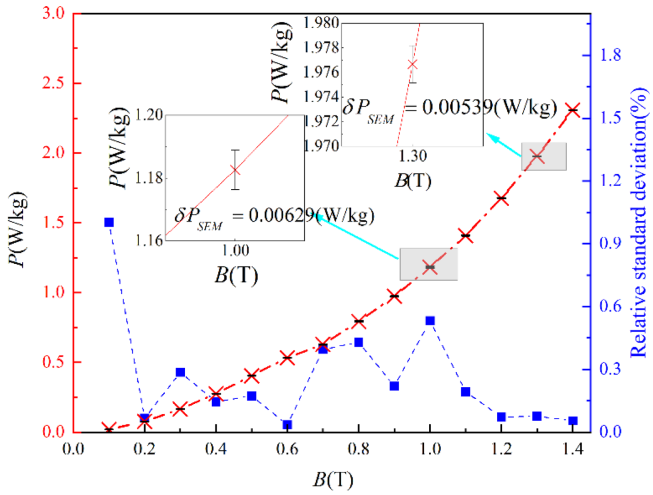

Fig. 5. (Color online) Standard deviation of loss in LLT repeatability testing.

$$\delta P_{SEM} = \sqrt{\frac{1}{(n-1)} \cdot \sum_{i=1}^{n}\left(P_{\text{ave}} - P_s^{(i)}\right)^2} \tag{3}$$

Here, P_{ave} represents the average loss of multiple measurements, $P_s(\mathrm{i})$ denotes the loss value for the ith measurement, and n represents the number of measurements. The relative standard deviation of losses is given by:

$$\delta P_{RSD} = \frac{\delta P_{SEM}}{P_{ave}} \times 100\% \tag{4}$$

As shown in Fig. 5, the curves of the mean and standard deviation of losses as functions of flux density are presented for the same position under different flux densities at an excitation frequency of 50 Hz. As can be seen from the figure, at the selected flux density points (1.0 T and 1.3 T), the standard deviations are relatively small, being 0.0062 W/kg and 0.0054 W/kg, respectively. The corresponding relative standard deviations of the losses are both less than 1%, indicating that the data measured by the LLT have good repeatability.

3.2. Motor stator loss measurement results and analysis

The Localized Loss Tester (LLT) is positioned at a

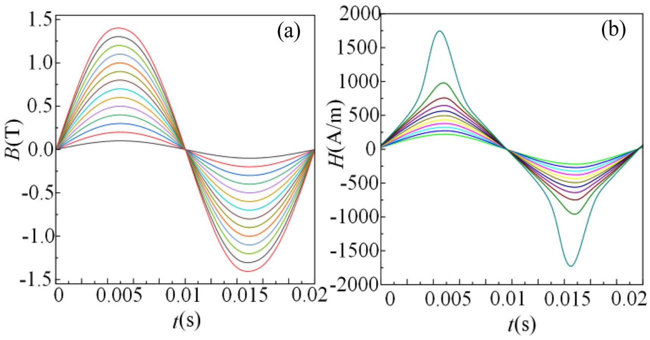

Fig. 6. (Color online) Time-domain waveform measurement results at different magnetic flux density peaks. (a) Magnetic flux density waveform. (b) Magnetic field strength waveform.

specific location on the electrical machine's stator core. To induce magnetization in the core region between the yoke poles, a 50 Hz alternating excitation current is applied to the excitation coil. Core losses are subsequently measured under preset magnetic flux density conditions. Crucially, all core loss and hysteresis loop data presented in this study were acquired under the condition of a sinusoidal magnetic flux density waveform. To ensure measuring repeatability, an iterative control method is employed to strictly maintain the form factor of the magnetic flux density waveform within 1.11±1%, corresponding to that of a standard sine wave [18, 19]. Fig. 6 presents B and H waveforms under varying flux density levels. Analysis of these waveforms reveals that as the magnetic flux density increases, the ferromagnetic core material approaches magnetic saturation. This state is characterized by the progressive alignment of internal magnetic domains. Consequently, the material's permeability decreases significantly, thereby requiring a substantial increase in the magnetic field strength to achieve further rises in flux density. This increased demand manifests as severe distortion in the magnetic field strength waveform, exhibiting characteristic peaking in the high-flux-density region.

Fig. 7 shows hysteresis loops at different frequencies. As the excitation frequency increases, the response time of the magnetic domains becomes insufficient to follow the rate of change in the magnetic field, causing an increase in hysteresis losses. Additionally, higher eddy current losses occur in the silicon steel at high frequencies. As hysteresis loss is proportional to the hysteresis loop area, this area increases with frequency.

To investigate the variation characteristics of stator tooth loss with angular position, core loss measurements were performed on the stator core at 20-degree intervals using an LLT, with the measurement configuration illustrated in Fig. 8(a). The measured data for each stator tooth were obtained by averaging ten repeated measurements. A digital iterative waveform control technique was employed to ensure that each measurement was conducted under identical peak magnetic flux density conditions. The measured loss results at peak magnetic flux densities of 0.6 T, 0.9 T, and 1.2 T at 50 Hz are presented in Figs. 8(b-d).

The measured core loss values at different angular positions under peak magnetic flux densities of 0.6 T, 0.9 T, and 1.2 T exhibit non-uniformly distributed. Instead, the losses exhibit a specific variation pattern with increasing angle: an initial increase is followed by a decrease, then a subsequent increase, and finally another decrease. This phenomenon primarily originates from the inherent magnetic anisotropy of the non-oriented silicon steel used in the stator core. Although non-oriented silicon steel is generally considered isotropic, its magnetic properties are influenced by the grain texture. The texture formed

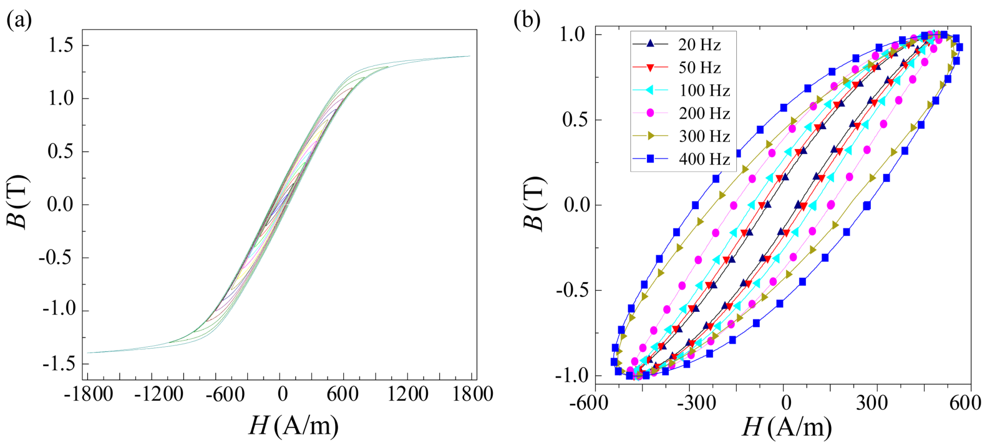

Fig. 7. (Color online) Hysteresis loop under alternating excitation (a) Hysteresis loops under different magnetic flux densities at 50 Hz. (b) Hysteresis loops at different frequencies.

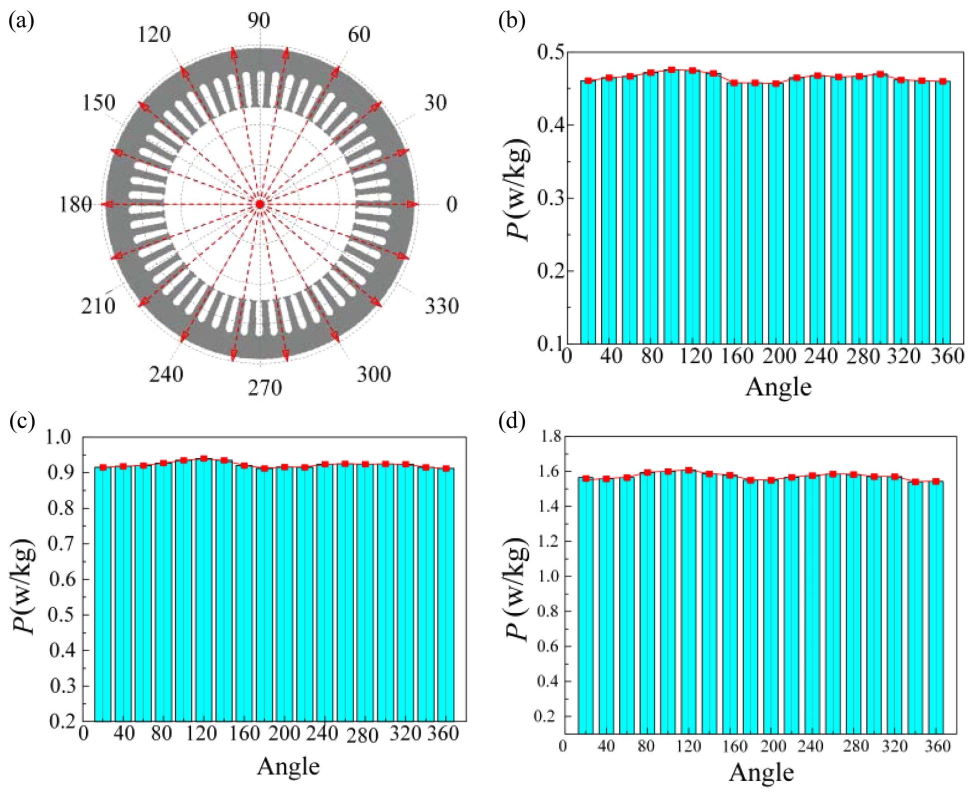

Fig. 8. (Color online) Loss characteristics from different angles (a) Different measurement angles of the stator core (b) Loss results at a magnetic flux density of 0.6 T (c) Loss results at a magnetic flux density of 0.9 T (d) Loss results at a magnetic flux density of 1.2 T.

during the rolling process leads to a higher concentration of crystallographic grains with easy magnetization axes aligned along the rolling direction, thereby enhancing the magnetic permeability in this direction. Accordingly, the magnetic characteristics of non-oriented silicon steel exhibit directional dependence, showing higher permeability along the rolling direction and lower permeability perpendicular to it. This anisotropy in permeability directly impacts the core loss characteristics at different angular orientations. Consequently, for this stator core, the rolling direction is defined as the 0° reference orientation, while the 90° direction corresponds to the axis perpendicular to the rolling direction. The loss distribution corresponding to different magnetic flux densities is shown in Fig. 9.

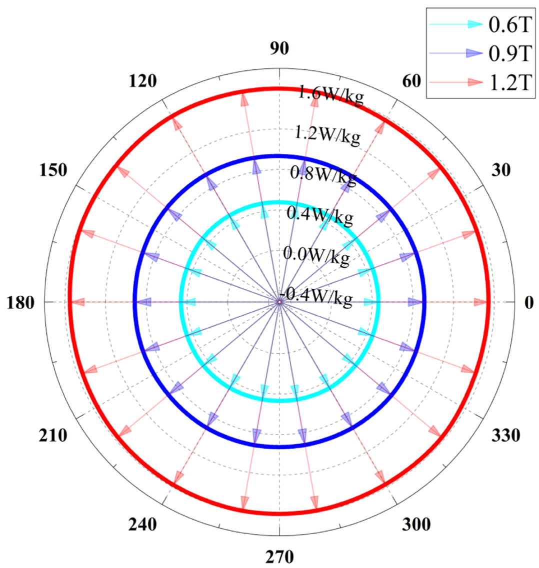

Fig. 9. (Color online) Distribution of losses on the stator core of the motor at 0.6 T, 0.9 T, and 1.2 T.

To characterize the axial distribution of magnetic properties in the stator core of an electric machine, systematic measurements were conducted at three characteristic axial locations: the edge zone, the quarter-point zone, and the central zone. As illustrated in Fig. 10, repeated measurements and comparative analyses of local magnetic properties were performed at each location. Test results demonstrate that, under 50 Hz fundamental-frequency AC excitation at a flux density of 0.8 T, the hysteresis loop morphology exhibits negligible variations across different depths. Minor fluctuations primarily arose from Gaussian

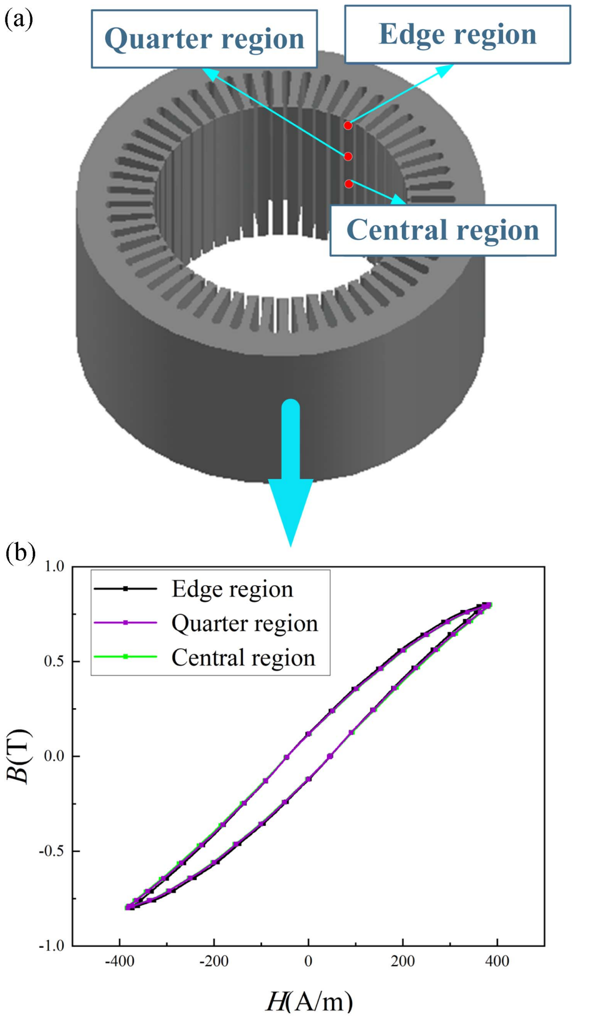

Fig. 10. (Color online) Comparison of hysteresis loops at different depths in the stator core of an electric motor (a) Measurement positions at different depths within the stator core of an electric motor (b) Comparison of hysteresis loops at different depths.

white noise interference within the measurement system, with a maximum recorded loss deviation of 0.002 W/kg. Therefore, the core has uniform magnetic properties along its axial direction.

As depicted in Fig. 11, a systematic comparison was conducted to assess the impact of residual stress on iron loss measurements, comparing the results from the SST method and the ring core method at a fixed magnetic flux density of 0.9 T. The analysis indicates that the iron loss values measured by the SST method are significantly lower than those measured by the ring core method, exhibiting an approximate 25% negative deviation. This discrepancy is attributed primarily to the residual stress suppression effect inherent in the SST method. Further comparative analysis confirms that the presence of

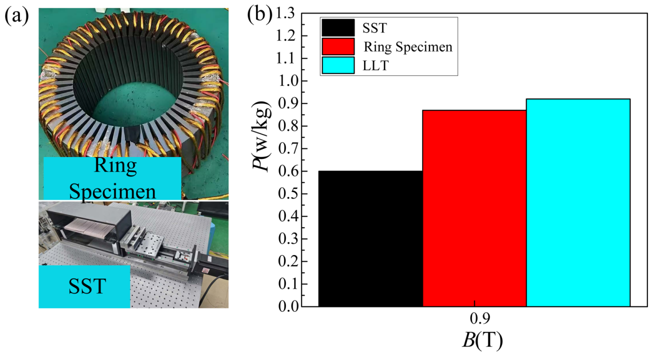

Fig. 11. (Color online) Comparison of losses at 0.9T using different measurement methods (a) Different loss measurement devices (b) Loss results measured by different devices.

residual stress leads to lower core loss values measured by the SST method relative to alternative methods.

Regarding the discrepancy observed between the ring core method and the LLT method, the key factor lies in their distinct measurement locations. Specifically, the ring core method predominantly assesses core loss within the stator yoke region, while the LLT method targets the stator tooth unit itself. Crucially, the stator tooth unit experiences more severe plastic deformation during the stamping process, resulting in higher residual stress levels. Consequently, this localized stress concentration significantly impacts the core loss values measured by the LLT method.

3.3. The effect of annealing on the loss of motor stator cores

During the manufacturing process of the stator core of an electric motor, the stamping process generates plastic strain in the stamping area. The stacking of laminations applies continuous compressive stress in the axial direction, while welding or bonding processes inevitably introduce thermal stress. Since the loss characteristics of

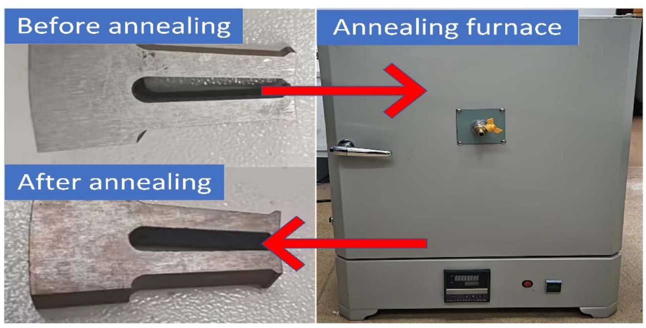

Fig. 12. (Color online) Annealed samples and schematic diagram of the annealing furnace.

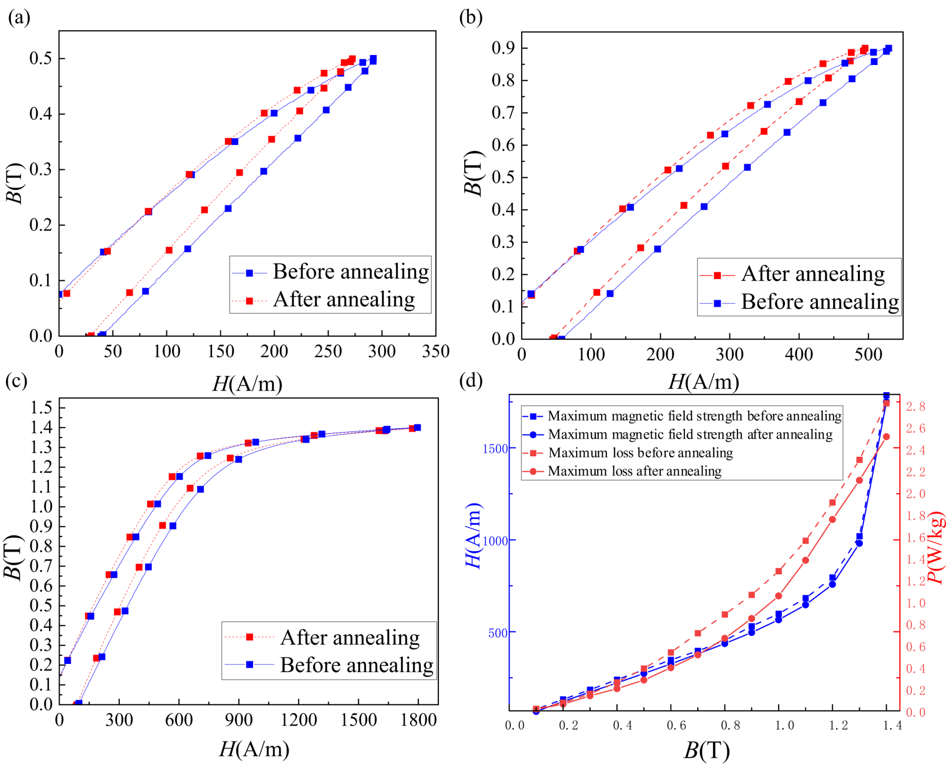

Fig. 13. (Color online) Comparison of magnetic properties of stator cores before and after annealing at different magnetic flux densities (a) Comparison at 0.5 T magnetic flux density (b) Comparison at 0.9 T magnetic flux density (c) Comparison at 1.2 T magnetic flux density (d) Comparison of core losses and peak magnetic field strength before and after annealing.

non-oriented silicon steel are susceptible to stress conditions, these mechanical stresses significantly alter the dynamic properties and spatial distribution of magnetic domains within the material, thereby affecting its electromagnetic performance.

To study the regulatory mechanism of annealing on soft magnetic properties, motor stator core specimens were fabricated from 20SW1200 silicon steel sheets with double-tooth unit structures. The variations in representative magnetic property parameters before and after annealing treatment were measured and compared using the developed core loss measurement apparatus. Structural details of the relevant physical specimens are presented in Fig. 12.

Fig. 13 presents comparative study of hysteresis loops measured under varying flux densities before and after

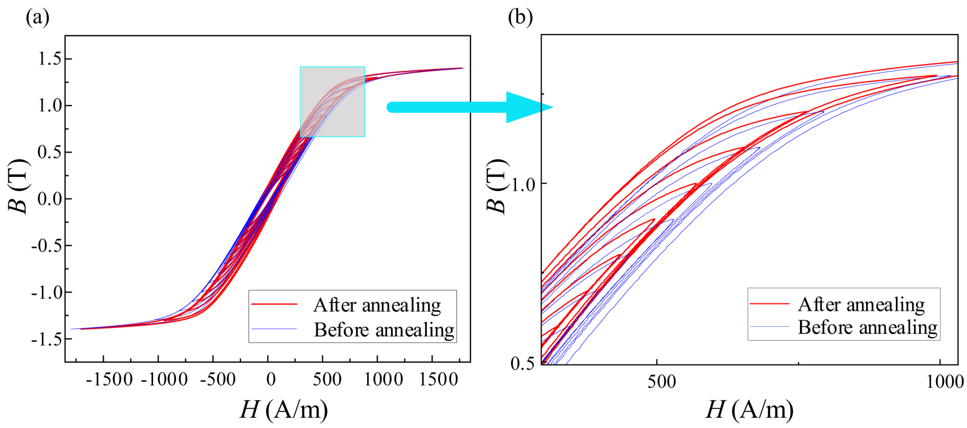

Fig. 14. (Color online) Comparison of hysteresis loops before and after annealing of stator cores at different magnetic flux densities (a) Global comparison (b) Local comparison.

stress-relief annealing. As depicted in Fig. 13(a), at a 0.5 T flux density, both the residual flux density (Br) and coercivity (Hc) exhibit a reduction post-annealing, accompanied by noticeable loop contraction. Consistent trends are observed in Figs. 13(b-c) at elevated flux densities. Quantitative analysis in Fig. 13(d) confirms a significant reduction in core loss after the annealing treatment. At 1.0 T flux density, core loss decreases by 0.214 W/kg (corresponding to a 20% reduction from pre-annealing values), with a concomitant 33 A/m reduction in peak magnetic field strength. The annealing process enhances the magnetic properties of silicon steel through multiple physical mechanisms: the elimination of residual stress fields, optimization of crystallographic texture orientation, refinement of grain size, reorganization of magnetic domain structures, and improvement of micro-structural morphology.

The comparative hysteresis loops of specimens before and after annealing treatment are presented in Fig. 14. It is observed that the hysteresis loop of the unannealed specimen exhibits a greater slope than that of the annealed specimen, suggesting lower permeability.

4. Conclusions

This paper presents a novel localized loss tester (LLT) for precise evaluation of motor stator core losses. This apparatus overcomes structural limitations of conventional testers, enabling high-resolution characterization of loss distribution at diverse internal positions. Obtained results demonstrated relatively uniform axial loss distribution, whereas significant circumferential variations were observed due to the magnetic anisotropy inherent in non-oriented silicon steel sheets. These spatial variations resulted in measurement deviations up to 25% for one-dimensional test methods. Comparative analysis revealed that stress-relief annealing effectively reduced Hc and Br, enhanced permeability, and suppressed residual stress-induced losses, yielding an approximate 20% reduction in total iron loss. The LLT serves as an effective tool for investigating localized loss mechanisms. The revealed characteristics (spatial loss distribution, material anisotropy, and annealing effects) contribute significantly to optimizing stator core design, refining manufacturing processes, and enhancing motor efficiency.

Acknowledgment

This work was supported by the National Natural Science Foundation of China under Grant No. 52477011 and No. 52207012.

References

[1] A. Dianov and A. Anuchin, IEEE Sens. J. **21**, 26488 (2021).
[2] K. D. M. Sousa, A. A. Hafner, H. J. Kalinowski, and J. C. C. da Silva, IEEE Sens. J. **12**, 3054 (2012).
[3] H. Shimoji, T. Ikeda, T. Todaka, S. Aihara, and K. Fujiwara, J. Magn. Magn. Mater. **591**, 171694 (2024).
[4] L. A. Kumar, B. M. Raj, and V. Vijayakumar, Sensors **20**, 6818 (2020).
[5] P. J. Banks and E. Rawlinson, Proc. IEE. **112**, 179 (1965).
[6] M. Shiozaki and Y. Kurosaki, Texture, Stress, Microstruct. **11**, 159 (1989).
[7] O. Hamrit, O. De la Barrière, M. LoBue, M. Lécrivain, and F. Mazaleyrat, Eur. Phys. J. Appl. Phys. **71**, 31001 (2015).
[8] Y. Kai, Y. Tsuchida, T. Todaka, and M. Enokizono, Int. J. Appl. Electromagn. Mech. **45**, 903 (2014).
[9] E. Brinksmeier, J. T. Cammett, W. König, P. Leskovar, J. Peters, and H. K. Tönshoff, CIRP Ann. **31**, 491 (1982).
[10] D. Sediako, J. Stroh, and S. Kianfar, Sci. Forum. **1016**, 1291 (2021).
[11] A. J. Clerc and A. Muetze, IEEE Trans. Ind. Appl. **48**, 1344 (2012).
[12] M. Oka and M. Enokizono, IEEE International Conference on Electrical Machines (ICEM) (2016) pp. 1344-1352.
[13] M. Oka, M. Enokizono, and Y. Mori, AIP Advances. **8**, 4 (2018).
[14] M. Oka, S. Kazunori, K. Makoto, and M. Enokizono, Materials Science Forum. **721**, 90 (2012).
[15] M. Oka, T. Ogasawara, N. Kawano, and M. Enokizono, IEEE Trans. Magn. **50**, 6300104 (2014).
[16] B. S. Abdel-Mageed, M. Ibrahim, J. Bhalala, and P. Pillay, IEEE Trans. Ind. Appl. **59**, 3278 (2023).
[17] J. P. Schlegel, N. Sadowski, N. J. Batistela, B. A. T. Iamamura, J. P. A. Bastos, and A. A. Espíndola, IEEE Trans. Magn. **48**, 715 (2012).
[18] L. Chen, X. Liu, T. Ben, D. Yan, and X. Zhang, AIP Adv. **14**, 025112 (2024).
[19] L. Chen, Hainan Huang, T. Ben, Biao Huang, and XianZhi Liu, J. Magn. **30**, 411 (2025).